Supporting information for

Low-Pressure PVD Growth SnS/InSe Vertical Heterojunctions with Type-II band Alignment for Typical Nanoelectronics

Peng Gao[a,bc,] Mengmeng Yang[a,b,c,] Chuanglei Wang[a,b,c,] Hengyi Li[a,b,c,] Baoxiang Yang[a,b,c,] Zhaoqiang Zheng[c], Nengjie Huo[a,b,c], Wei Gao[a,b,c*], Dongxiang Luo[a,b,d*], and Jingbo Li[a,b,c*]

[a] Institute of Semiconductors, South China Normal University, Guangzhou 510631, P. R. China.

[b] Guangdong Provincial Key Laboratory of Chip and Integration Technology, Guangzhou 510631, P. R. China.

[c] School of Materials and Energy, Guangdong University of Technology, Guangzhou 510006, P. R. China.

[d] Huangpu Hydrogen Innovation Center/Guangzhou Key Laboratory for Clean Energy and Materials, School of Chemistry and Chemical Engineering, Guangzhou University, Guangzhou 510006, P.R. China.

***Corresponding authors:** Wei Gao, Email: gaowei317040@m.scnu.edu.cn Dongxiang Luo, Email: luodx@gzhu.edu.cn Jingbo Li, Email: jbli@m.scnu.edu.cn

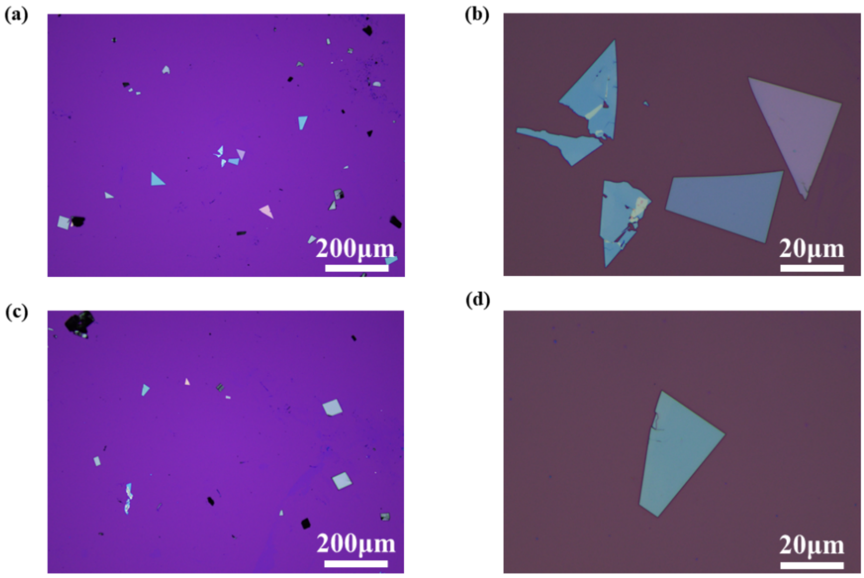

Figure S1. OM images of the SnS nanosheets prepared by LPPVD method. (a,c) OM images at the magnification of 10x.(b,d) OM images at the magnification of 100x.

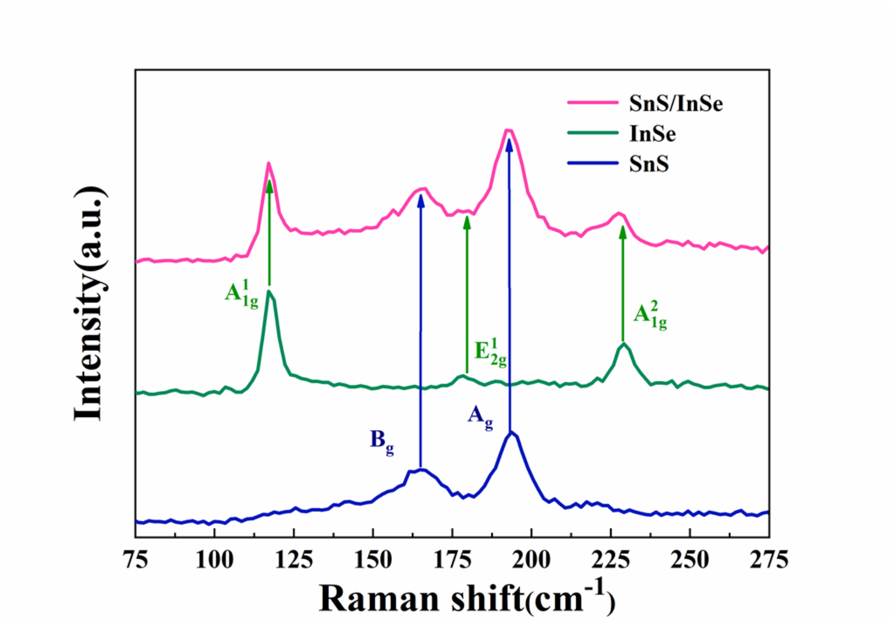

Figure S2. Raman Scattering spectra of individual SnS, InSe and their heterojunction for Device I.

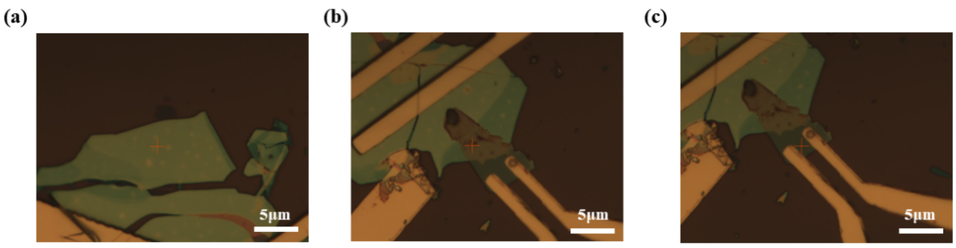

Figure S3. OM images for the device II in Raman spectra measurement (Figure 1c). (a) OM image of the chosen InSe.(b) OM image of the chosen SnS/InSe heterojunction. (c) OM image of the chosen SnS. The red cross represents the measured spot.

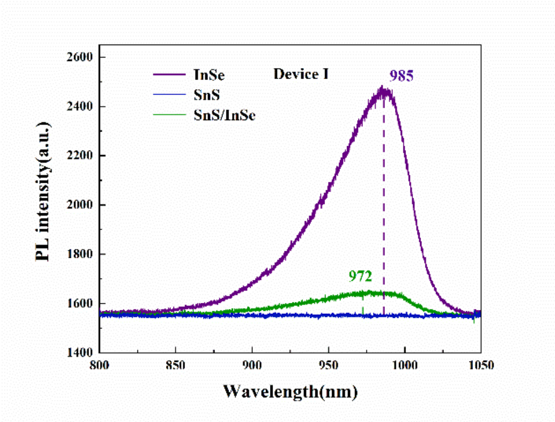

Figure S4. PL spectra of SnS, InSe and their heterojunction (Device I).

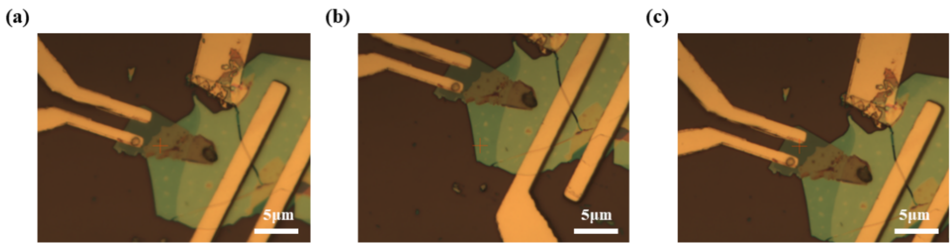

Figure S5. OM images for the device II in Photoluminescence measurement (Figure 1d). (a) OM image of the chosen InSe.(b) OM image of the chosen SnS/InSe heterojunction. (c) OM image of the chosen SnS. The red cross represents the measured spot.

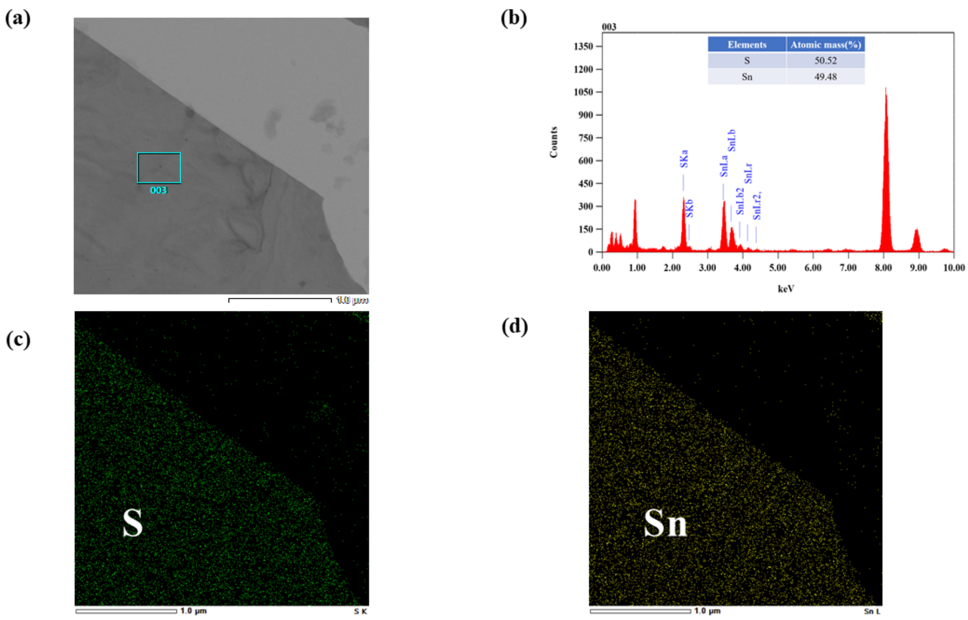

Figure S6. (a) HRTEM image and (b) The corresponding EDS spectrum and the extracted EDS data of SnS nanosheets in the blue square. (c,d) HRTEM EDS mapping of the elements S and Sn for the SnS nanosheet.

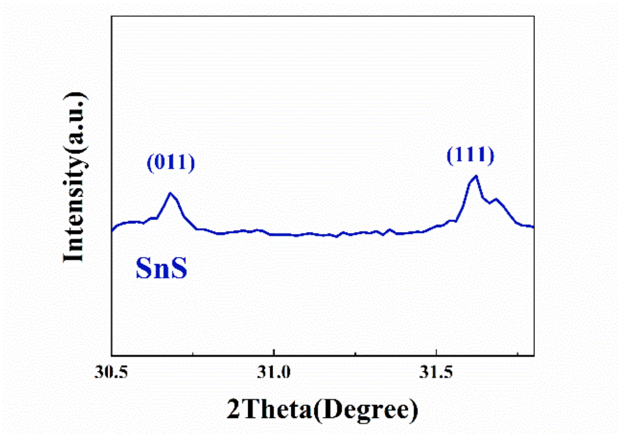

Figure S7. XRD patterns of SnS samples on SiO_2/Si substrates.

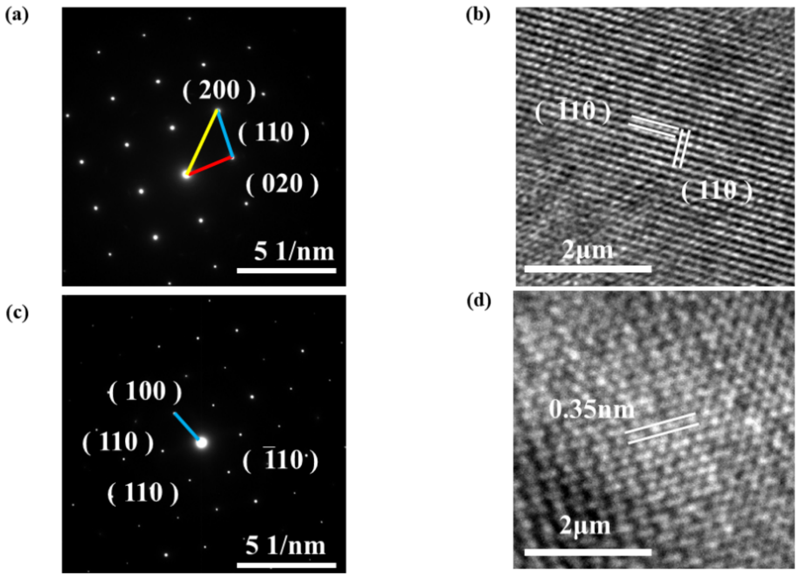

Figure S8. (a) selected area electron diffraction (SAED) pattern and (b)HRTEM image of the SnS nanosheet. (c) selected area electron diffraction (SAED) pattern and (d)HRTEM image of the InSe nanosheet.

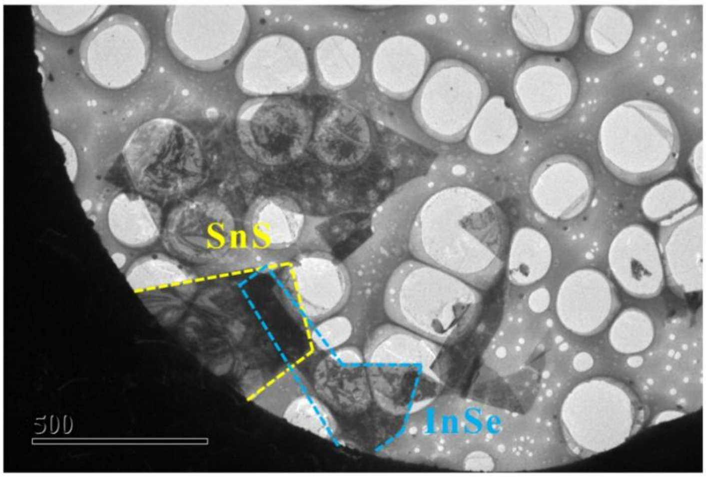

Figure S9. Low-resolution TEM image of the SnS / InSe heterojunction.

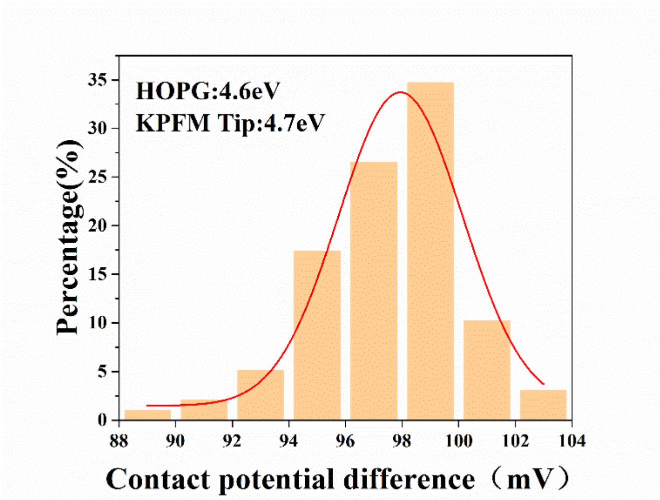

Figure S10. Histogram of contact potential difference of the HOPG surface.

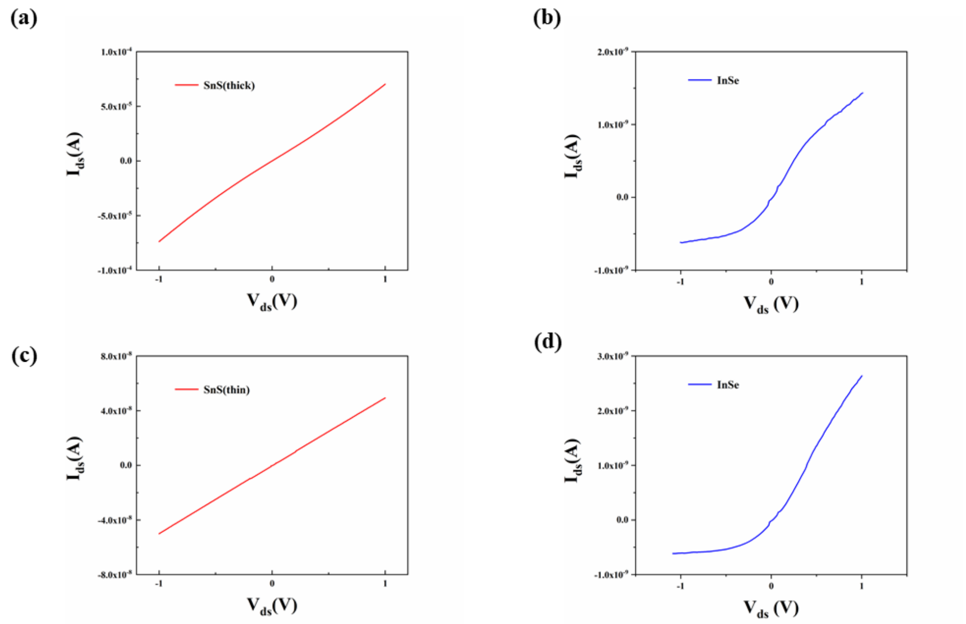

Figure S11. The electrical characteristics of individual FET. (a, b) the I-V curve of SnS(thick) and InSe of the device I under in dark conditions under ambient atmosphere, respectively. (c, d) the I-V curve of SnS(thin) and InSe of the device II under in dark conditions under ambient atmosphere, respectively.

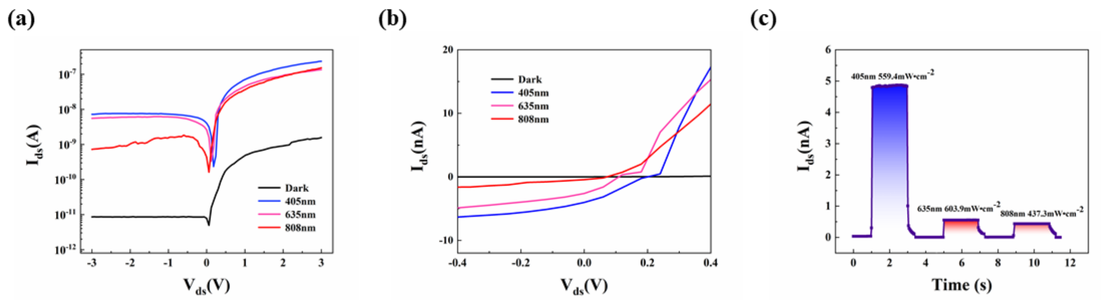

Figure S12. Logarithmic I_{ds}–V_{ds} curves of the device I under the wavelengths of 405 nm, 635 nm and 808 nm under darkness conditions. (b) The enlarged I_{ds}–V_{ds} curves of the device I under different wavelengths, showing the variation of the short circuit current (I_{sc}) and the open circuit voltage (V_{oc}). (c) Time-dependent photoresponse behavior of the the device I under different wavelengths at V_{ds} = 0 V.

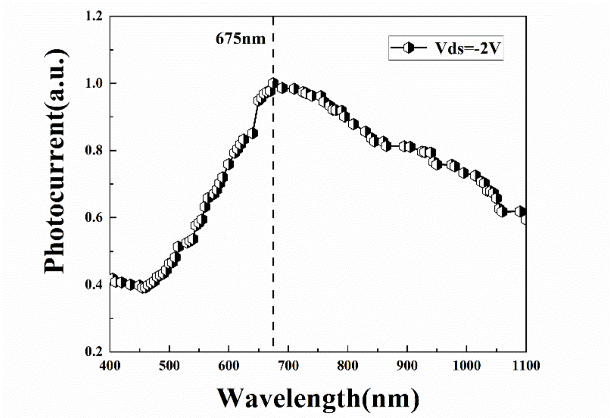

Figure S13. Wavelength-dependent relative responsivity of the device II at $V_{ds} = -2$ V.

Figure S14. The photolectric conversion efficiency (PCE) and Power dependent fill factor (FF) of the heterostructure device. The PCE can be calculated as:

$PCE = P_{el\,max}/P_{laser}$

And FF can be calculated as:

$FF = P_{max}/(I_{sc}V_{oc})$

where P_{max} is the maximum output electrical power.

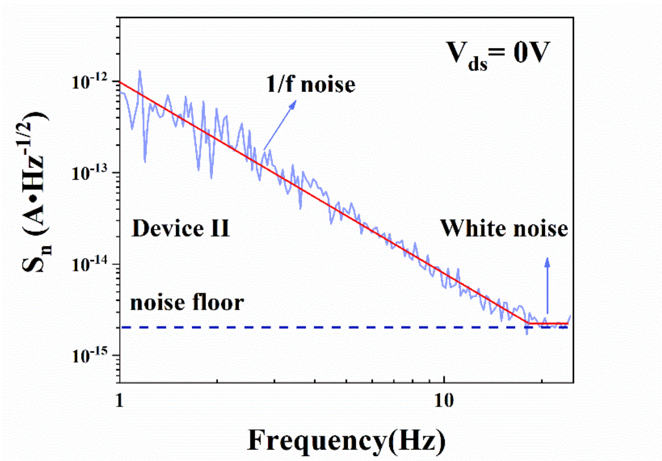

Figure S15. Noise spectral density (S_n) as a function of frequency at V_{ds}=0V.

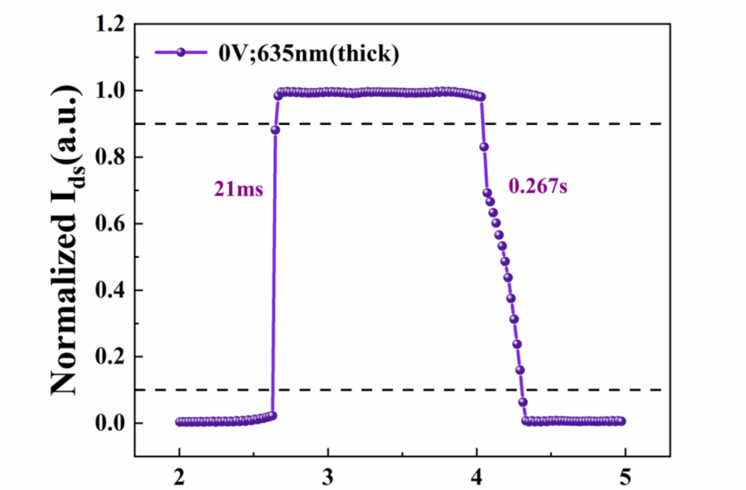

Figure S16. One cycle of the photoresponse of the device I to a wavelength of 635 nm at zero bias voltage for estimating both the rise and fall time.

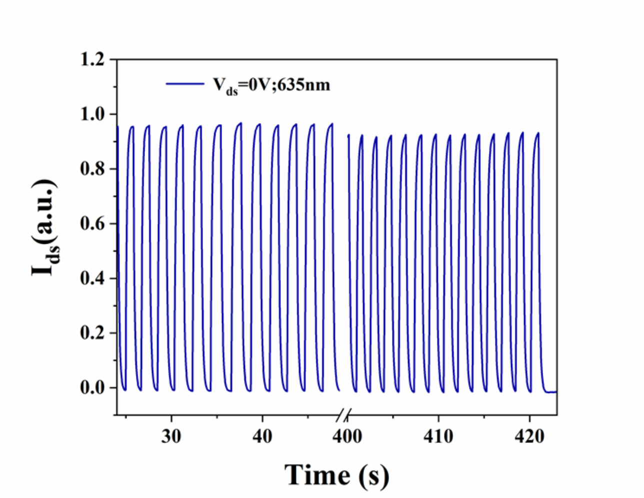

Figure S17. Four hundred seconds response behavior of the device II at V_{ds} = 0 V.

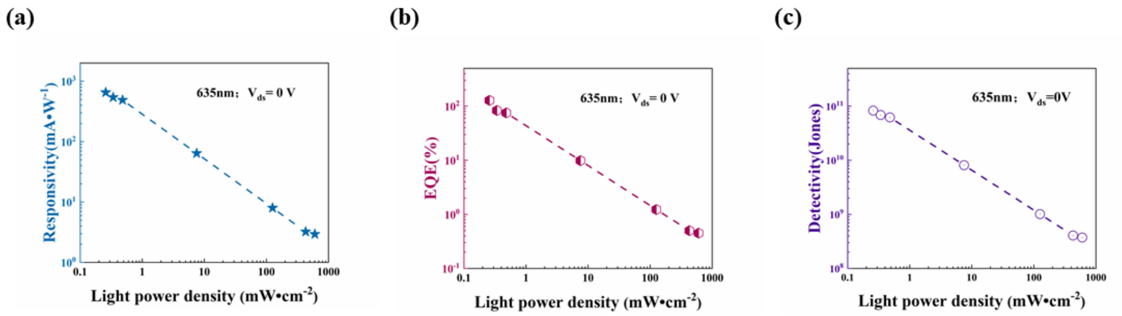

Figure S18. (a, b and c) Responsivity, EQE and detectivity of the device I as a function of light power density without bias.

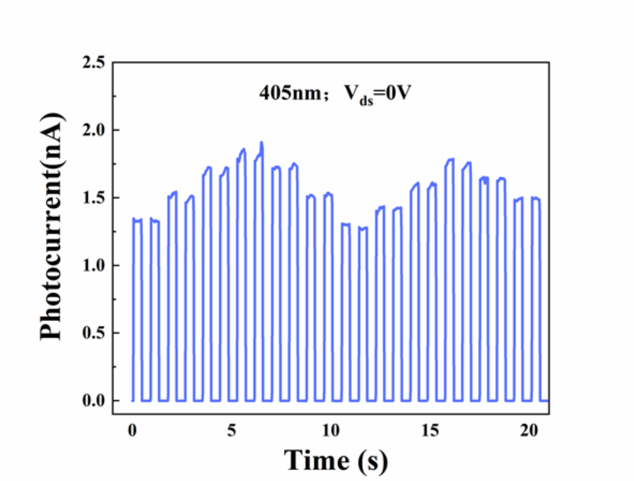

Figure S19. The time resolved photocurrent of the device II under polarized light with varying polarization angle from 0° to 330°under 635 nm light power.

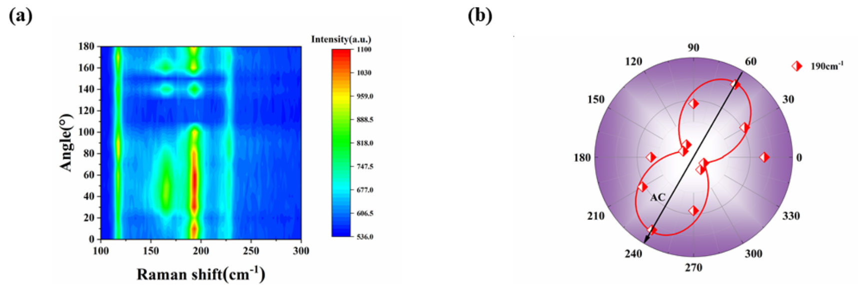

Figure S20. (a) Angle-resolved polarized Raman mapping of the device I as a function of polarization angle. b) Polar plots of Raman intensity with the Raman mode at 190 cm^{-1}, the pink line is the fitting curve.

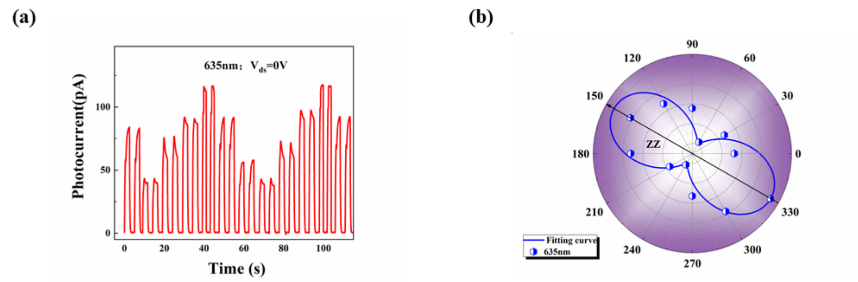

Figure S21. (a) The time resolved photocurrent of the device I under polarized light with varying polarization angle from 30° to 360°under 635 nm light power of 15.8 mW. (b) Polarizationsensitive photocurrent as a function of the polarization angle in the polar coordinates under linear-polarization laser of 635 nm at V_{ds} = 0 V.